Temperature Distribution And Mechanical Properties of FSW Medium Thickness 2219 Aluminum Alloy

Xiaohong Lu (lxhdlut@dlut.edu.cn)
Key Laboratory for Precision and Non-traditional Machining Technology of Ministry of Education
Yihan Luan
Dalian University of Technology
Xiangyue Meng
Dalian University of Technology
Yu Zhou
Dalian University of Technology
Ning Zhao
Dalian University of Technology
Steven Y. Liang
Georgia Institute of Technology

Research Article

Keywords: FSW, Temperature field, Mechanical properties, 2219 aluminum alloy, Medium thickness

Posted Date: August 26th, 2021

DOI: https://doi.org/10.21203/rs.3.rs-825845/v1

Version of Record: A version of this preprint was published at The International Journal of Advanced Manufacturing Technology on January 24th, 2022. See the published version at https://doi.org/10.1007/s00170-021-08505-1.

Temperature distribution and mechanical properties of FSW medium thickness 2219 aluminum alloy

a. Title of the manuscript

Temperature distribution and mechanical properties of FSW medium thickness 2219 aluminum alloy

b. Names, contact details and affiliation of all authors

1) The first and corresponding author: Professor Xiaohong Lu
Phone number: +86-15668685622; Email: lxhdlut@dlut.edu.cn
Affiliation: Key Laboratory for Precision and Non-traditional Machining Technology of Ministry of Education, Dalian University of Technology, 116024 Dalian, PR China.

2) The second author: Yihan Luan
Email: 1191449902@qq.com
Affiliation: Key Laboratory for Precision and Non-traditional Machining Technology of Ministry of Education, Dalian University of Technology, 116024 Dalian, PR China.

3) The third author: Xiangyue Meng
Email: 841061006@qq.com
Affiliation: Key Laboratory for Precision and Non-traditional Machining Technology of Ministry of Education, Dalian University of Technology, 116024 Dalian, PR China.

4）The forth author: Yu Zhou
Email: 3289245243@qq.com
Affiliation: Key Laboratory for Precision and Non-traditional Machining Technology of Ministry of Education, Dalian University of Technology, 116024 Dalian, PR China.

5) The fifth author: Professor Ning Zhao
E-mail: zhaoning@dlut.edu.cn
Affiliation: School of Materials Science and Engineering, Dalian University of Technology, 116024 Dalian, PR China.

6) The sixth author: Professor Steven Y. Liang
Phone number: 404-894-3200; Email: steven.liang@me.gatech.edu
Affiliation: The George W. Woodruff School of Mechanical Engineering, Georgia Institute of Technology, Atlanta, GA 30332-0405, U.S.A.

Temperature distribution and mechanical properties of FSW medium thickness 2219 aluminum alloy

Abstract

Friction stir welding (FSW) is a solid-state jointing technology, which has the advantages of high joint strength, low residual stress aXnd small deformation after welding. During the process of FSW, the welding temperature has an important effect on the quality of the weldment. Therefore, the heat generation model of FSW of medium thickness 2219 aluminum alloy is established based on the friction heat generation at the interface between the tool and the workpiece and the plastic deformation heat generation of the weldment material near the tool. The heat transfer model is set under the premise of considering heat conduction, thermal convection, and thermal radiation. Using JMatPro technology, the temperature-related material parameters of 2219 aluminum alloy are calculated based on the material composition, and the heat generation model is imported into the ABAQUS simulation software based on the DFLUX subroutine, and the establishment of the FSW thermodynamic model is realized. The effectiveness of the model is verified by FSW experiments. The thermodynamic model takes into account both heat generation (friction heat generation and plastic deformation heat generation) and heat transfer (heat conduction, thermal convection and thermal radiation), so it has a high prediction accuracy. Based on the FSW thermodynamic model, the influence of welding parameters on temperature distribution is explored, subsequently the influence of welding temperature on mechanical properties of welded joint are also studied. The research can provide guidance for predicting and characterizing the temperature distribution and the improvement of mechanical performance of FSW.

Keywords: FSW; Temperature field; Mechanical properties; 2219 aluminum alloy; Medium thickness

1. Introduction

To promote promote the leapfrog sustainable development of space technology and promote the study of major scientific issues such as the origin and evolution of life, manned moon landing and deep space exploration have become the responsibility of all countries to promote sustainable development. Manned moon landing and deep-space exploration have been included in the medium and long-term development plans of various countries, and the heavy launch vehicle is the basic vehicle. A certain heavy-lift launch vehicle storage tank has a diameter of 10 meters and a wall thickness of 18 mm. It is the main load-bearing structure of the rocket and has extremely high requirements for manufacturing quality and reliability. Friction stir welding (FSW) has become the main joining process for tank assembly due to its advantages such as pollution-free, smoke-free, no radiation, high welding efficiency, small product deformation after welding, and excellent weld mechanical properties [1].

FSW is a new type of solid-state jointing technology invented by the British Welding Research Institute in 1991 [2], which can realize flat seams, cylindrical circular seams, and spatial curved seams, and can complete butt joints, lap joints, T-joints, double Face welding and other welding methods, but to

ensure that the connection coefficient is not less than 0.7, it is still a challenge for FSW to weld 2219 aluminum alloy with a thickness of 18mm. The welding heat input is large, the welding high temperature time is long and the upper and lower temperature difference is large, the strengthening phase re-dissolution and the microstructure and properties of the weld are different in the thickness direction, which makes it difficult to obtain a high connection strength. It can be seen that the temperature distribution in the FSW process has a great influence on the welding quality [3]. In order to improve the connection strength of the weld, it is urgent to study the temperature distribution in the welding process.

At present, the research on FSW temperature field has mainly included experimental method, simulation method and analytical method. In the FSW process, it is difficult to directly obtain the temperature distribution over the weldment through experimental methods during the welding process due to the rotation of the tool, the shielding of the shoulder, the flow of the weldment material, and the severe plastic deformation. Using the finite element simulation method to study the temperature field has become an important means of analyzing the FSW process, but it cannot reveal the heat generation mechanism of the welding process. The analytical method can not only quickly obtain the temperature distribution of the weldment, but also reveal the heat generation mechanism of the FSW process. Therefore, the analytical method is used in this paper to study the FSW temperature field and further explore the influence of the temperature distribution on the mechanical properties of the FSW process. Relevant experts and scholars have conducted a lot of research on the modeling of FSW temperature using analytical methods. The heat source model of the FSW process was first described by the similar to Rosenthal analytical method of a uniformly moving point heat source or a linear heat source [4-5]. McClure et al. [4] used Rosenthal analysis method in 1998 to conduct a preliminary analysis of heat transfer in the FSW process. Since the weldment is assumed to be the heat conduction problem of a semi-infinite object, the accuracy of the simulation results is not high, but the proposal of this method opens up a new way for the study of the FSW temperature field. Later, Song and Kovacevic [6] also established the FSW heat source model based on the Rosenthal analytical method, but ignored the heat generation by plastic deformation. With the in-depth study of the analytical FSW heat source model, Chang et al. [7] established a heat source model considering the frictional heat generation of the tool shoulder, the tool pin, and the weldment, simulated the temperature field of the 4mm thick 6061-T6 aluminum alloy FSW, and studied the effect of welding speed on the microhardness and tensile strength of welded joints. Frigaard et al. [8] established a heat source model based on the frictional heat generation of torque, used MATLAB code to simulate the temperature distribution of 6mm thick AA6082-T6 and AA7108-T79 weldments and analyzed the microhardness of the weldment material according to the prediction model, but the heat source model ignored the heat generated by plastic deformation. Kiral et al. [9] used the same torque heat source model as Frigaard et al. and used ANSYS and HyperXtrude software to simulate the temperature field of the 3.1mm thick 6061-T6 aluminum alloy FSW, and investigated the effect of

different rotational speed, welding speed, and dwell time on the peak temperature of the weldments. Schmidt et al. [10] considered the different contact conditions between the tool and the weldment, the concave angle of the shoulder and the cone angle of the tool pin, and modified the heat source model. Gadakh[11], Yaduwanshi[12], Ghetiya[13], Liu W M[14], Bonifaz[15], Liu X Q[16] based on Schmidt's heat source model, separately studied the effects of rotational speed and welding speed, axial pressure, cone angle of the tool pin, backing plate type and welding inclination angle on the temperature distribution of thin plates. Among them, Ghetiya's research showed that the tensile strength and microhardness of joints are affected by temperature.

Analytical FSW heat source models have been studied in great depths, but some FSW heat source models have only considered the frictional heat generation of the tool, while ignoring the heat generated by the plastic deformation of the weldment material during the welding process, which leads to errors in the prediction of the temperature field. Moreover, research studies have been basically carried out around low-strength thin plates, but there are few studies on high-strength medium plates. Compared with low-strength thin plates, the temperature and mechanical properties of high-strength medium thickness plates are more uneven in the FSW process [17], and the welding quality is difficult to guarantee. Therefore, there is an urgent need to establish an FSW heat source model that considers friction heat generation and plastic deformation heat generation, and explores the temperature distribution of the 2219 aluminum alloy plates of medium thickness, so as to provide a deeper understanding of the welding process performance and weld quality.

2. FSW thermodynamic model

The FSW process generates heat through friction, softens the welding material, and mixes the material through the stirring action of the tool pin. The main mechanism of the FSW process is the contact interactions between the tool6 pin and the shoulder and the weldment material. The shoulder is the main source of heat generated by friction. Another function of the shoulder is to keep the material flowing around the tool. The tool pin is located below the shoulder, and its main function is to mix the sheet materials to be welded. In fact, in the FSW process of the plate material, heat is generated by not only the friction between the tool and the sheet material, but also the plastic deformation in the stirring zone. In the FSW process, the heat is generated by various sources and also by various types of complex heat transfer processes: namely the heat conduction, thermal convection and thermal radiation. The FSW process is a complex thermodynamic and heat transfer process.

2.1 Heat production model

The tool moves in the processing direction while rotating at a high speed. Frictional heat is generated between the tool and the welded plates due to the existence of frictional resistance. The heat during welding comes from the frictional heat between the tool and the welded plate, including the friction heat Q_1 between the shoulder and the surface of the welded plate, the friction heat Q_2 between

the side of the tool pin and the welded plate, and the friction heat Q_3 between the bottom surface of the tool pin and the welded plate. The welded plate near the tool will produce plastic deformation under the action of the tool, and these plastic deformations will also generate heat Q_t.

The friction heat Q_1 between the shoulder and the surface of the welded plate :

$$Q_1 = \omega \int_{R_2}^{R_1} dM_1 = \frac{2\pi\mu p\omega}{3}\left(R_1^3 - R_2^3\right) \quad (1)$$

$$dM_1 = r_1 df = 2\pi p\mu r_1^2 dr_1 \quad (R_2 \le r_1 \le R_1) \quad (2)$$

Where μ is the friction coefficient, p is the positive pressure, ω is the rotation speed of the tool, R_1 is the shoulder radius, R_2 is the large diameter of the tool pin, R_3 is the small diameter of the tool pin, dM_1 is the micro-element torque of the shoulder, and df is the micro-element friction.

The frictional heat Q_2 between the side of the tool pin and the welded plate:

$$Q_2 = \omega \int_{O}^{H} dM_2 = \frac{2\pi\mu p\omega}{3\sin\alpha}\left(R_2^3 - R_3^3\right) \quad (3)$$

$$dM_2 = rdf = 2\pi p\mu (R_3 + h\tan\alpha)^2 \frac{dh}{\cos\alpha} \quad (4)$$

Where H is the length of the tool pin, 2α is the cone angle of the tool pin, and dM_2 is the micro-element torque on the side of the tool pin.

The friction heat Q_3 between the bottom surface of the tool pin and the welded plate :

$$Q_3 = \omega \int_{0}^{R_3} dM_3 = \frac{2\pi\mu p\omega}{3} R_3^3 \quad (5)$$

$$dM_3 = rdf = 2\pi p\mu r^2 dr \quad (6)$$

Where dM_3 is the micro-element torque of the bottom surface of the tool pin.

Plastic deformation heat Q_t:

$$Q_t = \eta_p \bar{\sigma} \dot{\varepsilon}_p \quad (7)$$

Where η_p is the conversion coefficient of plastic deformation energy into thermal energy, $\bar{\sigma}$ is the equivalent stress, and $\dot{\varepsilon}_p$ is the equivalent strain rate.

Therefore, the total heat production Q_{total} during the FSW process should equal the sum of the friction heat Q_1, Q_2, Q_3 and the plastic deformation heat Q_t.

$$Q_{total} = Q_1 + Q_2 + Q_3 + Q_t \quad (8)$$

2.2 Heat transfer model

The FSW process is very complicated, and the temperature of the weldment material changes all the time, so the three-dimensional transient heat transfer problem is analyzed. Assuming that the heat conduction of the material is isotropic, in the Cartesian coordinate system, the transient temperature field

$T(x,y,z,t)$ in the deformed body satisfies the differential equation:

$$\rho c\frac{\partial T}{\partial t}-\lambda\left(\frac{\partial^2 T}{\partial x^2}+\frac{\partial^2 T}{\partial \mathrm{y}^2}+\frac{\partial^2 T}{\partial \mathrm{y}^2}\right)-\dot{Q}=0 \quad (9)$$

Where ρ is the material density; c is the specific heat capacity of the material; t is the time; λ is the thermal conductivity of the material; $\dot{Q}$ is the heat source density inside the object.

The accuracy of the temperature field in the FSW process is related to heat input on one hand, and heat output on the other hand. When the tool rotates at a high speed and is pressed into the welded plate frictional heat is generated due to the friction between the tool and the welded plate. As the tool presses down to a certain position on the welded plate, tool starts to move in the welding direction. There is a great temperature gradient between the tool and welded plate, so that the heat is transferred from the high temperature area to the low temperature area. The main transfer methods are heat conduction, thermal convection, and thermal radiation.

(1) Heat conduction

The temperature difference within an object or system is a necessary condition for heat conduction. The rate of heat conduction is determined by the distribution of the temperature field in the object. Heat conduction follows Fourier's law, and its basic form is:

$$q=\text{-}\lambda\frac{\partial T}{\partial x} \quad (10)$$

Where q is the heat flux density, λ is the thermal conductivity of the material, and $\frac{\partial T}{\partial x}$ is the temperature gradient in the direction of heat conduction.

In the FSW process, there is heat conduction between the tool and the welded plate, the inside of the welded plate, and between the welded plate and the fixture and the backing plate as follows.

①The heat conduction between the tool and the welded plate

In FSW process, a lot of heat is generated due to the frictional resistance between the tool and the welded plate. The total heat generated will have a certain distribution ratio between the tool and the welded plate, and the distribution ratio can be different, depending on the model.

②The heat conduction inside the welded plate

Heat will first be generated from the area where the tool directly acts on the welded plate. Subsequently, heat will be transferred from the high temperature area in the welded plate to the low temperature area because of the temperature difference between this area and the surrounding welded plate. The rate of heat transfer depends on the thermal conductivity of the welded plate.

③The heat conduction between welded plate and backing plate

When the thermal boundary conditions are considered, the thermal conductivity of the contact area between the welded plate and the backing plate, that is, the bottom surface of the welded plate, is set to 100W/(m^2·K) [18].

(2) Thermal convection

Usually the Newtonian cooling formula is used to describe the thermal convection:

$$q = h\Delta T \tag{11}$$

Where q is the heat flux density; h is the coefficient of heat convection, and ΔT is the temperature difference between solid and fluid.

In the FSW process, the coefficient of heat convection on the upper surface and the four sides of the weldment is set as 30W/(m^2·K) [18].

(3) Thermal radiation

Thermal radiation refers to the heat exchange process in which an object absorbs electromagnetic energy emitted by other objects and converts it into heat. Thermal radiation does not require a heat transfer medium. The radiant heat flux can be calculated using the empirical correction formula of Stephen-Polzman's law.

$$Q = \varepsilon F \sigma_b T^4 \tag{12}$$

Where Q is the heat flux, T is the absolute temperature, ε is the emissivity, F is the surface area, and σ_b is the thermal radiation constant.

2.3 Material parameters

XRF-1800 X-ray fluorescence spectrometer is used to determine the material composition of 2219 aluminum alloy. The material composition is shown in Table 1. Use JMatPro software to import material composition calculation to obtain material parameters that change with temperature, as shown in Fig. 1.

Table 1 Composition of 2219 aluminum alloy (wt%)

Cu	Mn	Fe	Si	Zn	V	Ti	Zr	Mg	Al
6.21	0.29	0.12	0.15	0.06	0.08	0.03	0.12	0.02	Bal

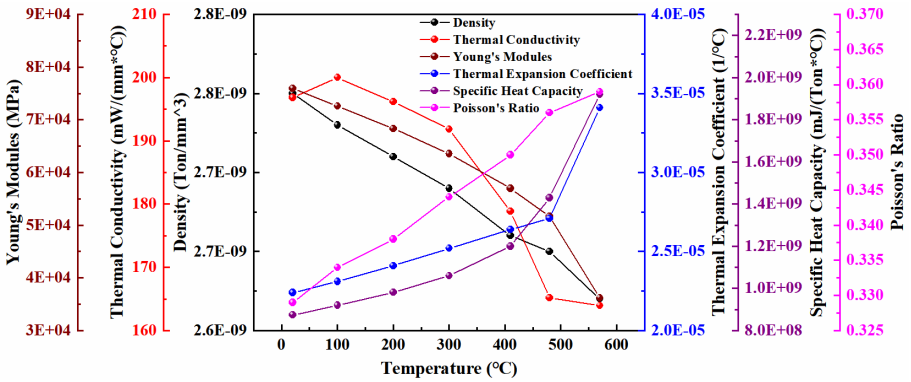

Fig. 1 The material parameters of 2219 aluminum alloy

During the FSW process, the weldment undergoes violent elastoplastic deformation. The strain and strain rate of the weldment change greatly. To accurately describe this characteristic of the weldment in the FSW process, Johnson-Cook constitutive model is adopted as expressed by the following formula:

$$\sigma = \left(A + B\varepsilon^{n}\right)\left(1 + C\ln\frac{\dot{\varepsilon}}{\dot{\varepsilon}_0}\right)\left[1 - \left(\frac{t - t_r}{t_m - t_r}\right)^{m}\right] \quad (13)$$

Where σ is the flow stress; A is the plastic strain; B is the strain rate; C is the reference plastic strain rate; t is the temperature of the weldment; t_m is the melting temperature of the weldment material; t_r is the room temperature. A, B, C, m and n are material parameters, where A is the yield strength, B is the hardening modulus, C is the strain rate sensitivity coefficient, n is the hardening coefficient, and m is the thermal softening coefficient.

Parameters of Johnson-Cook constitutive of 2219 aluminum alloy are shown in Table 2 [19].

Table 2 Johnson-Cook constitutive model parameters of 2219

A (MPa)	B (MPa)	n	C	m
170	228	0.31	0.028	2.75

2.4 Coefficient of friction

When the tool pin is in contact with the weldment interface, formulas (1), (3), (5), (8) fully describe the heat generated by the FSW process, and the use of a rationality of the friction coefficient is to ensure that the heat generation model is a correct foundation. In the FSW process of aluminum alloy, the friction coefficient decreases with the increase of welding temperature. Therefore, it is necessary to adopt temperature-dependent adaptive adjustment of the friction coefficient (as shown in Table 3) to better express the heat generation model. In the numerical calculation, it is realized by adjusting the value of μ in each time step *dt,* so that the welding temperature will have a steady state, instead of increasing the temperature as the welding progresses.

Table 3 Friction coefficient related to temperature [18]

Temperature（℃）	25	300	420	543
Friction coefficient	0.3	0.25	0.2	0.01

2.5 Implementation of thermodynamic model

Based on the DFLUX subroutine, the heat generation model is imported in the ABAQUS simulation software, and the FSW thermodynamic model is completed by combining the heat transfer model, the material parameters of the 2219 aluminum alloy and the friction coefficient. When the speed is 400rpm and the welding speed is 100mm/min, the solution of the final temperature field is shown in Fig. 2.

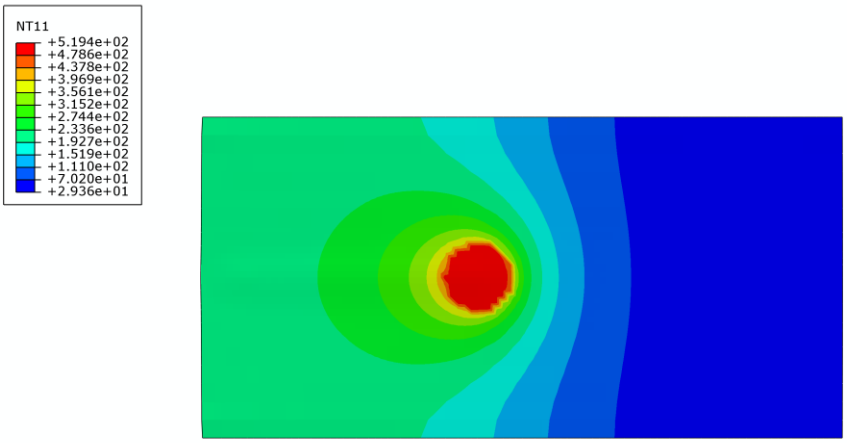

Fig. 2 FSW temperature field

3. Experimental verification of FSW thermodynamic model

The welding temperature in the FSW process is used to experimentally verify the validity of the established thermodynamic model for FSW of 2219 aluminum alloy.

3.1 FSW experimental conditions

A gantry type FSW machine tool is used to carry out the FSW experiment, as shown in Fig. 3. The FSW temperature field test system based on K-type thermocouple is used to detect the welding temperature field. The temperature measurement range is 0-1000℃, the measurement error is 0.75%T, and the sampling frequency is 10Hz. The welding material is 2219 aluminum alloy plate of 300mm*75mm*18mm. The diameter of the shoulder of the tool is 32mm, the diameter of the large end of the tool pin is 15mm, the diameter of the small end is 7mm, and the length of the tool pin is 17.8mm, as shown in Fig. 4.

Fig. 3 Large-scale gantry type friction stir welding equipment

Fig. 4 Tool for welding

The experimental parameters of FSW are set as follows: the welding speed is 100mm/min, the plunge rate is 20mm/min, and the rotational speeds are 350rpm, 400rpm and 450rpm, respectively.

The tensile test is carried out on the electronic universal testing machine DNS-300. The sample size is in accordance with GB/T228.1-2010. The schematic diagram of the sample is shown in Fig. 5, and the tensile rate is set to 2mm/min. The electronic Brinell hardness tester HBS-3000 is used to measure the microhardness distribution of FSW welded joints. The loading time in the test is 30s, and the distance between every two measuring points is 10mm. Use the German MEF-4 metallurgical microscope to observe the microstructure of the joint. A field emission scanning electron microscope (SUPRA55) with energy dispersive spectroscopy (EDS) function is used to scan the tensile fracture.

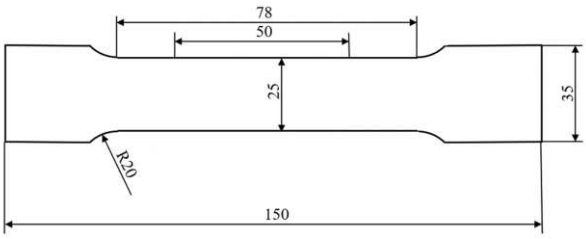

Fig. 5 Schematic diagram of tensile specimen

3.2 Model verification

To verify the effectiveness of the simulation model, characteristic points are selected on the 2219 aluminum alloy sheet for temperature curve comparison. Fig. 6 shows a schematic diagram of the characteristic points of the thermocouple embedded in the FSW temperature measurement experiment. The characteristic points are 15mm, 18mm, 21mm from the center of the weldment and 6mm from the surface of the weldment.

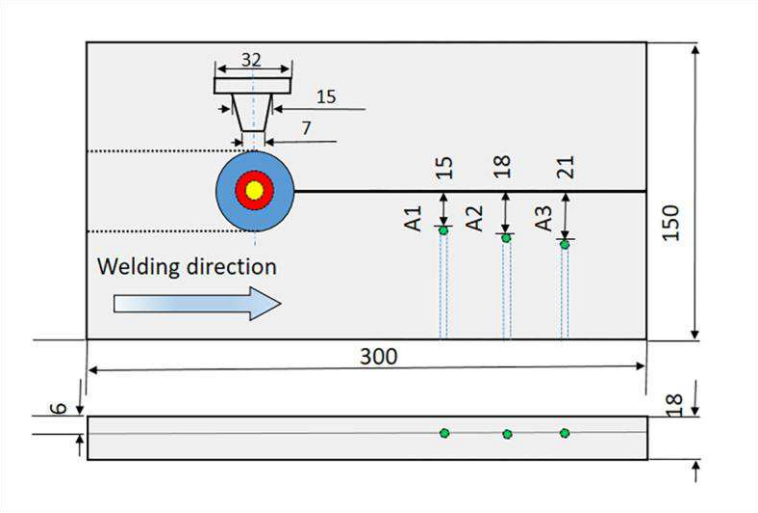

Fig. 6 Location of thermocouples in FSW

When the spindle speed is 400rpm and the welding speed is 100mm/min, the temperature comparison between the simulated value of characteristic temperature points A1, A2, A3 and the experimental value is shown in Fig. 7, 8, and 9.

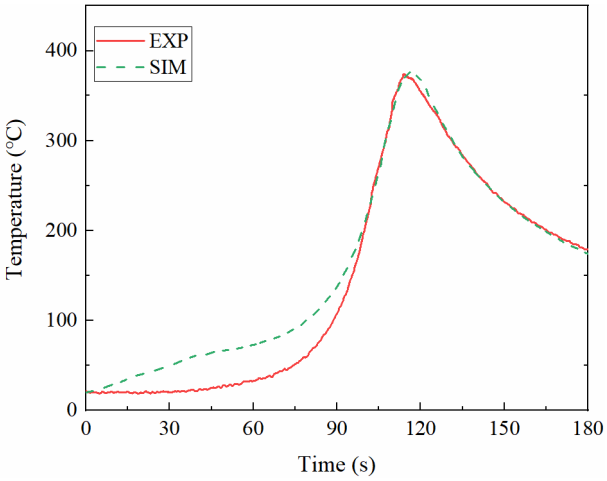

Fig. 7 Temperature curve between simulated and experimental values at A1

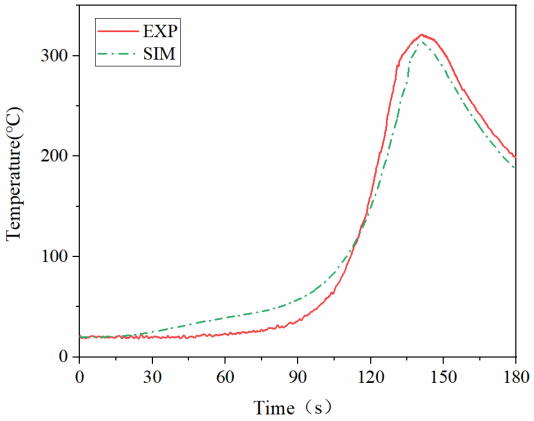

Fig. 8 Temperature curve between simulated and experimental values at A2

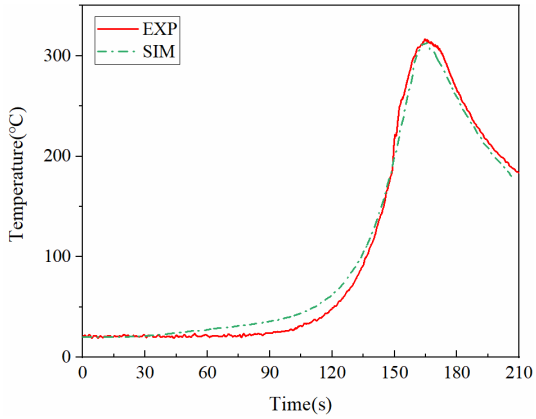

Fig. 9 Temperature curve between simulated and experimental values at A3

Table 4 Comparison of simulation output and experimental results

Position	Experimental peak temperature （℃）	Simulated peak temperature （℃）	Error （%）
A1	373.9	376.3	0.6
A2	320.9	315.1	2
A3	314.5	316.7	0.7

The comparison results of the simulation output and the experimentally measured welding temperature are shown in Fig. 7, 8, and 9. The characteristic temperature point temperature output by the FSW thermodynamic model based on the analytical method is close to the experimentally measured temperature. Table 4 shows that the maximum relative error of peak temperature is 2%, and the average relative error of peak temperature is 1.1%, which verifies the validity of the established 2219 aluminum alloy FSW thermodynamic model.

4. Results and discussion

In the FSW process, the welding speed and the rotational speed of the tool are two important process parameters. The selection of different process parameters affects the temperature distribution of the weldment, subsequently the distribution of the temperature field has a direct impact on the mechanical properties of the welded joint. Because of the existence of the tool in the FSW process, the temperature of each position of the weld cannot be obtained, the required temperature is obtained through the FSW thermodynamic model as discussed herein.

4.1 Welding temperature

At the center of the joint line and 6mm away from the upper surface of the weldment, model computations have been performed to capture the effect of different welding speeds on the temperature when rotational speed is 400rpm, and the effect of different rotational speeds on the temperature when the welding speed is 100mm/min, as shown in Fig. 10 and Fig. 11.

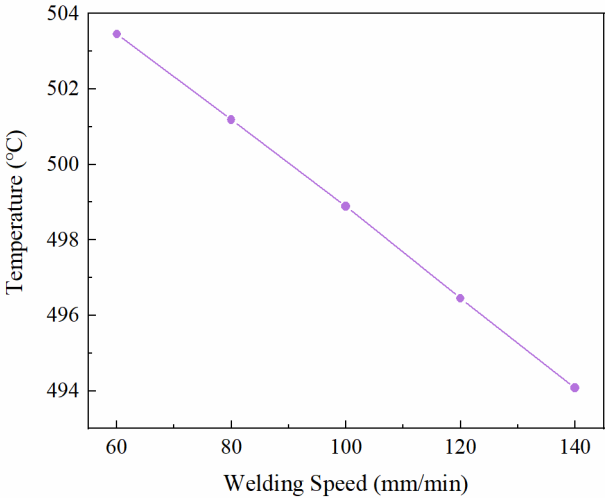

Fig. 10 Peak temperature at different welding speeds

Table 5 Peak temperature values at different welding speeds

Welding Speed (mm/min)	60	80	100	120	140
Temperature (℃)	503.5	501.2	498.9	496.4	494.1

When the rotational speed is 400rpm and the welding speeds are 60, 80, 100, 120 and 140mm/min, the peak welding value temperature is 503.5, 501.2, 498.9, 496.4 and 494.1℃, respectively, as shown in Table 5. As shown in Fig. 10, while the welding speed increases the welding temperature gradually decreases. This is because of the fact that as the welding speed increases, the frictional heat generation time shortens, the unit heat flux density becomes smaller, and the welding temperature decreases.

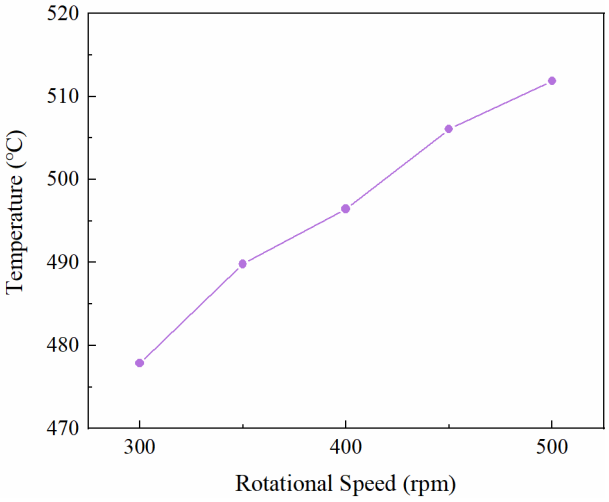

Fig. 11 Peak temperature at different rotational speeds

Table 6 Peak temperature values at different rotational speeds

Rotational Speed (rpm)	300	350	400	450	500
Temperature (℃)	477.9	489.8	498.9	506.6	511.9

When the welding speed is 100mm/min and the rotational speeds are 300, 350, 400, 450 and 500rpm respectively, the welding value temperature is 477.9, 489.8, 498.9, 506.6 and 511.9℃, as shown in Table 6. As shown in Fig. 11, the welding temperature gradually increases as the rotational speed of the welding tool increases. The physical reason could be understood as follows: with the

increase of the rotational speeds, the value of ω increases, the heat generation of Q_1, Q_2, and Q_3 in formulas (1), (3), (5) increases, so the welding temperature rises.

4.2 Mechanical properties of joints

In the FSW process, because the temperature field is not uniformly distributed, the welded joint is subjected to different temperatures, resulting in differences in microhardness. To facilitate the study of the mechanical properties of the welded joint, the heat-affected zone (HAZ), the thermo-mechanically affected zone (TMAZ), the nugget zone (NZ) and the [20] are evaluated. The grain-level microstructure of each zone is shown in Fig. 13. As shown in Fig. 12 with the "0" point being the center of the joint line, where NZ is located, the microhardness of the FSW joint of 2219 aluminum alloy with 18 mm thickness is roughly “U” shape. The mean microhardness of NZ zone is 285HB, slightly higher than the mean microhardness (281HB, 284HB) of the two sides of NZ. This is because in the vertical weld direction, the welding temperature gradually decreases from the joint line center to both sides, that is, the temperature of the NZ is higher than that of the TMAZ and the HAZ, and the grain structure has undergone dynamic recrystallization, forming fine equiaxed grains (as shown in Fig. 13(a)), which may increases the microhardness. However, as heat input in the TMAZ and HAZ is lower, the crystal grains grow, the microhardness is then slightly lower than that in the NZ. As can be seen in Fig. 11, the welding temperature of FSW increases with the rotational speed, but the microhardness of the NZ microhardness is 295 HB when the rotational speed is 400 rpm (when the welding temperature is 498.9℃). This microhardness value reaches 77% of the microhardness of the matrix metal (383 HB).

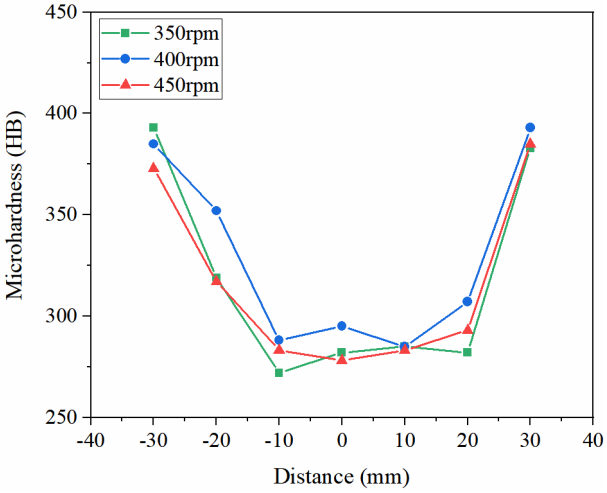

Fig.12 Microhardness distribution

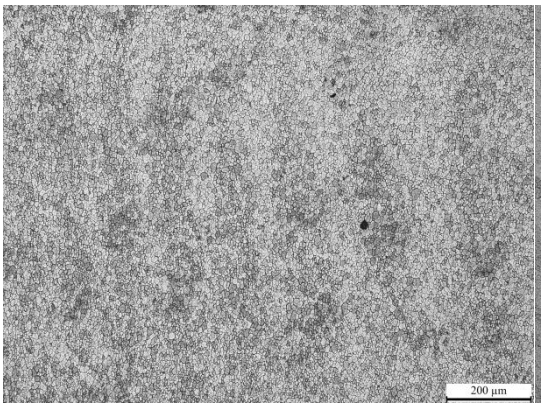

Fig. 13(a) Microstructure of NZ

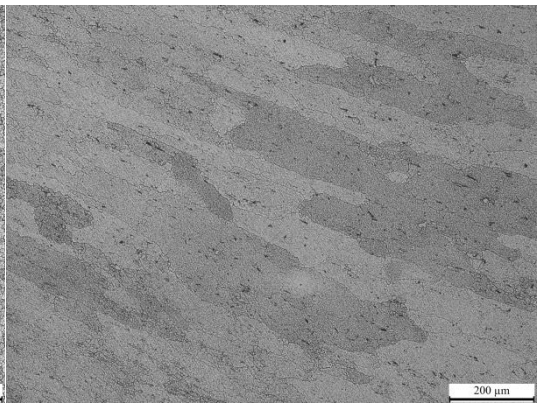

Fig. 13(b) Microstructure of TMAZ

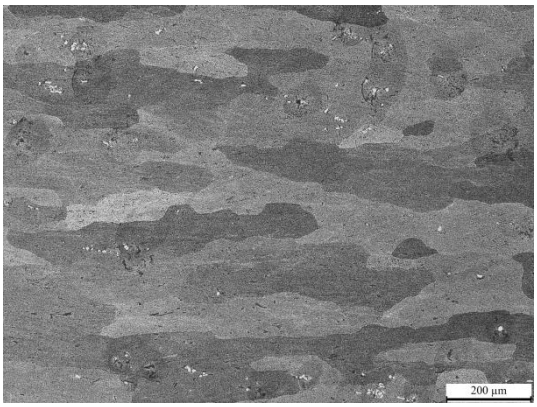

Fig. 13(c) Microstructure of HAZ

Fig. 13 Microstructure of joint

The 18mm thick 2219 aluminum alloy FSW welded joint is cut in the crown, midplane and root three layers along the vertical direction of the weld, with each layer having a thickness of 6mm. The welding speed is 100mm/min, and the rotational speed of the tool is 350, 400, and 450rpm, respectively. Fig. 14 shows the results of the tensile test of the welded joint. The tensile strength of each layer increases first and then decreases. The maximum tensile strength of the crown at 400rpm is 315MPa, which reaches 72.4% of the matrix metal's tensile strength (435MPa), while the elongation rate is 3.3%. When the rotational speed of the tool is 450 rpm, the overall tensile strength decreases. It can be seen from Fig. 15 that the rule of tensile strength in the thickness direction can be understood as follows: the tensile strength of the crown is the highest, followed by the midplane and the root. The possible reason is that the microstructure affected by temperature and in turn affects the tensile strength of the joint. It can be seen from Fig. 15 that the crown has the highest temperature, stronger thermal cycling effect, stronger dynamic recrystallization degree, and significantly improved joint tensile strength; the midplane and root have relatively lower temperatures, and the dynamic recrystallization degree decreases, resulting in a lower tensile strength. The 6005A-T6 aluminum alloy, which is also 18mm thick, has obtained a welded joint with a tensile strength of 81.0% of the matrix metal's tensile strength in the joint tensile performance test [21]. The tensile strength of the welded joint of 2219 aluminum alloy is only 72.4% of the tensile

strength of the base material. This is mainly due to the high strength of 2219 aluminum alloy, the large axial force required for welding, the high heat input obtained, and the uneven distribution of the welding temperature of medium plate, which leads to large differences in the internal structure and properties of the joints. These effects are evident in the “S” lines of oxide accumulation in the NZ, as shown in Fig. 16. As the grains of the NZ grow, the oxides in the "S" line hinder the migration of grain boundaries and produces stress concentration, which makes the tensile strength of the joint.

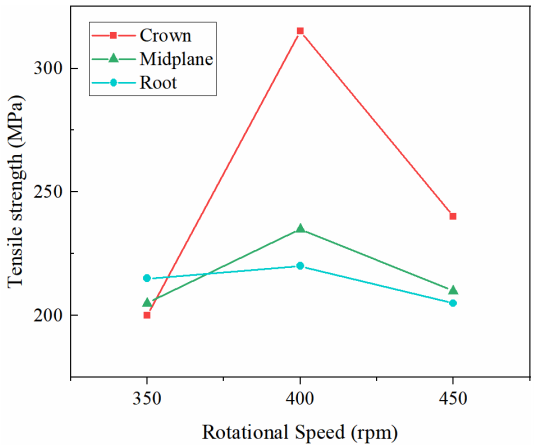

Fig. 14 Tensile test results of welded joints

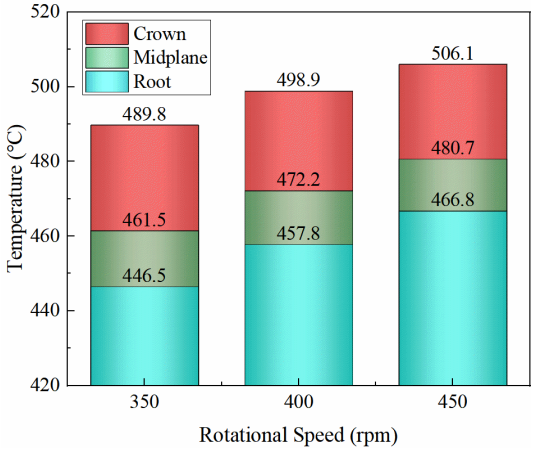

Fig. 15 Temperature distribution of welded joints

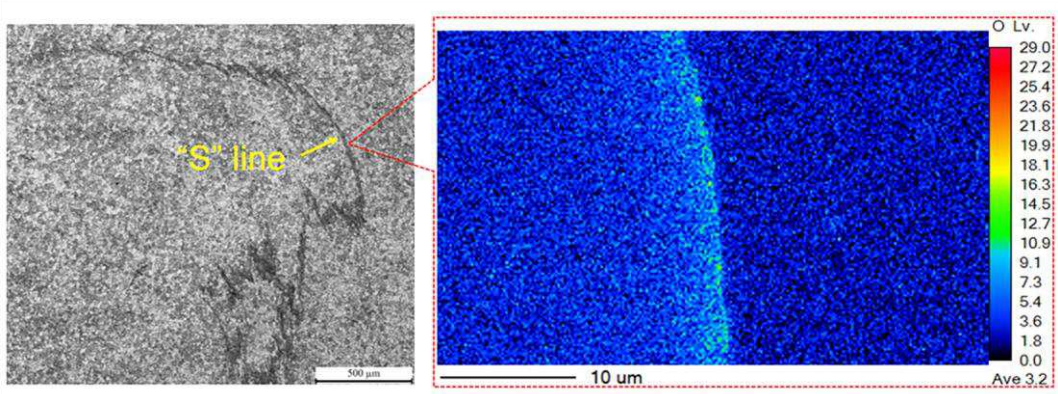

Fig. 16 “S” line distribution of welded joints

The macroscopic fracture morphology of the joint is shown in Fig. 17(a). The fracture positions of the joints are all located in the NZ. The scanning electron microscope of the fracture surface of the joint is shown in Fig. 17(b). It can be seen that the fracture surface of the joint presents dimples of different sizes with deep pores. The average diameter of the large dimples is about 14.2μm, and the diameter of the small dimples is about 14.2μm. There are a large number of strengthening phase particles at the bottom of the dimples. In order to analyze the composition of the strengthening phase particles, EDS is performed on the particles. The EDS results show that the particle composition is Al_2Cu, and the presence of the strengthening phase particles is beneficial to the tensile strength of the joint. It implies that the fracture form of the joint is ductile fracture, indicating that the welded joint has good toughness. However, the tensile test results show that the fracture location is at the NZ, but in the tensile test of the thin 2219 aluminum alloy, the fracture position is located at the junction of NZ and TMAZ [22]. The possible reason is that the internal temperature of thick 2219 aluminum alloy is not evenly distributed along the thickness direction during FSW process, which leads to the uneven distribution of the strengthening phase Al_2Cu, therefore the overall tensile strength of the joint is not high.

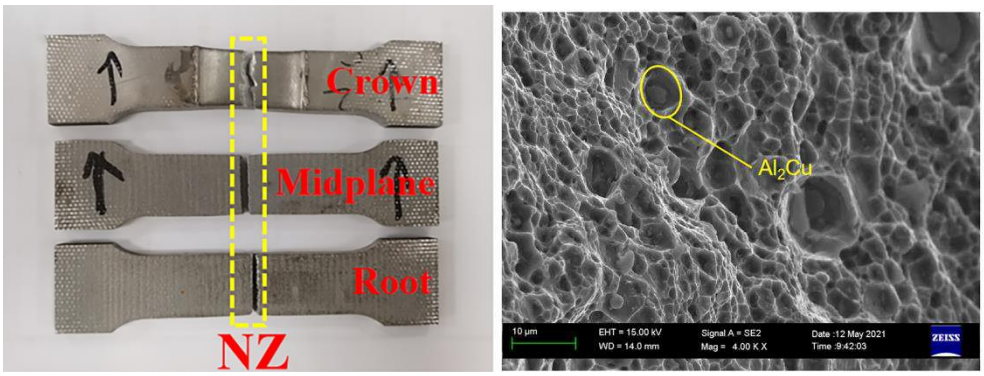

Fig. 17(a) Fracture macroscopic morphology **Fig. 17(b)** SEM of joint fracture morphology

Fig. 17 Fracture morphology of joint

5. Conclusion

In this paper, a heat generation model of 2219 aluminum alloy FSW is established based on the frictional heat generation of the tool and the plastic deformation heat generation of the weldment material. The heat transfer is set up based on the considerations of heat conduction, thermal convection, and thermal radiation. Based on the DFLUX subroutine, the heat generation model is imported into the ABAQUS simulation software, and the establishment of the FSW thermodynamic model is realized. The effectiveness of the model is verified by FSW experiments over a range of process parameters. The maximum relative error between the predicted results and the experimental results is limited to 2%, and the mean relative error is 1.13%. Based on the FSW thermodynamic model, the influence of welding parameters on temperature is explored. Results show that the welding temperature decreases with the increase of welding speed, and the welding temperature increases with the increase of rotational speed. The rule of tensile strength in the thickness direction can be characterized as follows: the tensile strength of the crown is the highest, followed by the midplane and the root. When the rotational speed is 400rpm (the welding temperature is 498.9℃ at this time), the microhardness of the NZ is 295HB, which reaches 77% of the microhardness of the matrix metal. Similarly, when the rotational speed is 400rpm, the tensile strength of the crown weldment material reaches the maximum value of 315MPa, which is 72.4% of the matrix metal's tensile strength, and the elongation rate is 3.3%. The fracture form of the joint is observed to be ductile fracture, and Al_2Cu is a strengthening phase particle in the dimple. The unevenness distribution of temperature, the unevenness distribution of strengthening phase Al_2Cu and the existence of “S” line during FSW lead to the benefits in the mechanical properties of the joint. The research results could provide guides for the predicting and characterizing the temperature distribution and mechanical performance of rocket tank FSW.

References

[1] Chen J, Shi L, Wu C, Jiang Y (2021) The Effect of Tool Pin Size and Taper Angle on the Thermal Process and Plastic Material Flow in Friction Stir Welding. Int J Adv Manuf Technol https://doi.org/10.21203/rs.3.rs-335152/v1

[2] Sarikavak Y (2021) An advanced modelling to improve the prediction of thermal distribution in friction stir welding (FSW) for difficult to weld materials. Journal of the Brazilian Society of Mechanical Sciences and Engineering 43:4. https://doi.org/10.1007/s40430-020-02735-2

[3] Hidetoshi F, Sun Yufeng, Hideaki K (2011) Microstructure and mechanical properties of friction stir welded pure Mo joints. Scr Mater 64(7):657-660. https://doi.org/10.1016/j.scriptamat.2010.12.014

[4] McClure J C, Tang W, Murr L E, Gould J E (1998) A Thermal Model of Friction Stir Welding//ASM Proceedings of the International Conference: Trends in Welding Research 590-595.

[5]Russell M J, Shercliff H R (1999) Analytical modelling of friction stir welding. In: Russell MJ, Shercliff R, editors. INALCO'98: seventh international conference on joints in aluminium. Cambridge, UK: TWI; 197–207.

[6]Song M, Kovacevic R (2003) Thermal modeling of friction stir welding in a moving coordinate system and its validation. Int J Adv Manuf Technol 43(6): 605-615. https://doi.org/10.1016/S0890-6955(03)00022-1

[7] Chang W S, Bang H S, Jung S B, Yun MY, Lee WB (2003) Joint properties and thermal behaviors of friction stir welded age hardenable 6061Al alloy//Materials Science Forum. Trans Tech Publications Ltd., Zurich-Uetikon, Switzerland, 426: 2953-2958.
https://doi.org/10.4028/www.scientific.net/MSF.426-432.2953

[8] Frigaard O, Grong O, Midling O T (2001) A process model for friction stir welding of age hardening aluminum alloys. Metall Mater Trans A Phys Metall Mater Sci 32(5): 1189-1200.
https://doi.org/10.1007/s11661-001-0128-4

[9] Kiral B G, Tabanolu M, Serindag H T (2013) Finite element modeling of friction stir welding in aluminum alloys joint. Mathematical and Computational Applications 18(2): 122-131.
https://doi.org/10.3390/mca18020122

[10] Schmidt H, Hattel J, Wert J (2004) An analytical model for the heat generation in friction stir welding[C]. Model Simul Mat Sci Eng 12(1): 143-157.
https://doi.org/10.1088/0965-0393/12/1/013

[11] Gadakh V S, Adepu K (2013) Heat generation model for taper cylindrical pin profile in FSW. Journal of Materials Research and Technology 2(4): 370-375.
https://doi.org/10.1016/j.jmrt.2013.10.003

[12] Yaduwanshi D K, Bag S, Pal S (2015) Heat transfer analyses in friction stir welding of aluminium alloy. Proc Inst Mech Eng B J Eng Manuf 229(10): 1722-1733.
https://doi.org/10.1177/0954405414539297

[13] Ghetiya N D, Patel K M (2018) Numerical simulation on an effect of backing plates on joint temperature and weld quality in air and immersed FSW of AA2014-T6. Int J Adv Manuf Technol.
https://doi.org/10.1007/s00170-018-2632-3

[14] Liu W M, Yan Y F, Sun T, Wu S , Shen Y (2019) Influence of cooling water temperature on ME20M magnesium alloy submerged friction stir welding: a numerical and experimental study. Int J Adv Manuf Technol 105(12): 5203-5215.
https://doi.org/10.1007/s00170-019-04496-2

[15] Bonifaz E A (2019) A new thermal model in SAE-AISI 1524 friction stir welding. Defect and Diffusion Forum 390: 53-63.
https://doi.org/10.4028/www.scientific.net/DDF.390.53
[16] Liu X Q, Yu Y, Yang S L, Liu H J (2020) A Modified Analytical Heat Source Model for Numerical Simulation of Temperature Field in Friction Stir Welding. Advances in Materials Science and Engineering. https://doi.org/10.1155/2020/4639382
[17] Canaday C T , Moore M A , Wei T, Reynolds A P (2013) Through thickness property variations in a thick plate AA7050 friction stir welded joint. Materials Science & Engineering A 559: 678-682. https://doi.org/10.1016/j.msea.2012.09.008
[18] Aziz S B, Dewan M W, Huggett D J, et al (2018) A fully coupled thermomechanical model of friction stir welding (FSW) and numerical studies on process parameters of lightweight aluminum alloy joints. Acta Metallurgica Sinica 31(1): 1-18.
https://doi.org/10.1007/s40195-017-0658-4
[19] ZHANG Zi-qun, JIANG Zhao-liang, WEI Qing-yue (2017) Dynamic Mechanical Properties and Constitutive Equations of 2219 Aluminum Alloy. Journal of Materials Engineering 45(10): 47-51.
https://doi.org/10.11868/j.issn.1001-4381.2016.000859
[20] Batool A, Anjum N A, Khan M Y (2021) Impact of pin tool designs on the mechanical properties and microstructure of aluminum alloys AA7075-AA6061. Journal of the Chinese Institute of Engineers : 1-11.
https://doi.org/10.1080/02533839.2021.1940293
[21] MENG Teng-yi, DENG Qing-hong, YOU Fei, WU Yong, CHEN Kai (2020) Research on single-side high speed friction stir welding of 6005A-T6 aluminum alloy thick plate. Welding Technology 49(10): 43-46.
https://doi.org/10.13846/j.cnki.cn12-1070/tg.2020.10.014
[22] He D, Zhao Z, Lai R, et al (2018) Research on the Microstructure and Mechanical Properties of Ultrasonic Assisted Friction Stir Welding Joints of 2219-T87 Aluminum Alloy. Journal of Hunan University Natural Sciences 45(4): 41-47.
https://doi.org/10.16339/j.cnki.hdxbzkb.2018.04.006

Figure captions

Fig. 1	The material parameters of 2219 aluminum alloy
Fig. 2	FSW temperature field
Fig. 3	Large-scale gantry type friction stir welding equipment
Fig. 4	Tool for welding
Fig. 5	Schematic diagram of tensile specimen
Fig. 6	Location of thermocouples in FSW
Fig. 7	Temperature curve between simulated and experimental values at A1
Fig. 8	Temperature curve between simulated and experimental values at A2
Fig. 9	Temperature curve between simulated and experimental values at A3
Fig. 10	Peak temperature at different welding speeds
Fig. 11	Peak temperature at different rotational speeds
Fig. 12	Microhardness distribution
Fig. 13	(a) Microstructure of NZ (b) Microstructure of TMAZ (c) Microstructure of HAZ Microstructure of joint
Fig. 14	Tensile test results of welded joints
Fig. 15	Temperature distribution of welded joints
Fig. 16	“S” line distribution of welded joints
Fig. 17	(d) Fracture macroscopic morphology (e) SEM of joint fracture morphology Fracture morphology of joint

Table captions

Table 1	Composition of 2219 aluminum alloy (wt%)
Table 2	Johnson-Cook constitutive model parameters of 2219
Table 3	Friction coefficient related to temperature
Table 4	Comparison of simulation output and experimental results
Table 5	Peak temperature values at different welding speeds
Table 6	Peak temperature values at different rotational speeds

Declarations

Funding

The research was supported by the National Key Research and Development Program of China (Grant No. 2019YFA0709003), Dalian Science and Technology Innovation Fund (Grant No. 2020JJ26GX041) and the Fundamental Research Funds for the Central Universities (Grant No. DUT20ZD204. The financial contributions are gratefully acknowledged.

Conflicts of interest/Competing interests

Not applicable. The authors declare that they have no conflict of interest.

Availability of data and material

All data generated or analysed during this study are included in this manuscript.

Code availability

The code is available on request.

Authors' contributions

Xiaohong Lu: Conceptualization, Supervision, Methodology, Funding acquisition, Project administration.
Yihan Luan: Conceptualization, Methodology, Software, Validation, Writing - original draft, Investigation, Writing - Review & Editing.
Xiangyue Meng: Formal analysis, Data Curation.
Yu Zhou: Software, Investigation.
Ning Zhao: Formal analysis.
Steven Y. Liang: Resources.

Ethics approval

Not applicable

Consent to participate

Not applicable

Consent for publication

The authors consent that the work entitled as “Temperature distribution and mechanical properties of FSW medium thickness 2219 aluminum alloy” for possible publication in International Journal of Advanced Manufacturing Technology.